Ceres Evolution and current state

Mc Cord T., C. Sotin

▶ **To cite this version:**

Mc Cord T., C. Sotin. Ceres Evolution and current state. Journal of Geophysical Research, 2005, 110 (E5), pp.CiteID EO5009. 10.1029/2004JE002244 . hal-00116029

HAL Id: hal-00116029
https://hal.science/hal-00116029

Submitted on 12 Feb 2021

HAL is a multi-disciplinary open access archive for the deposit and dissemination of scientific research documents, whether they are published or not. The documents may come from teaching and research institutions in France or abroad, or from public or private research centers.

L'archive ouverte pluridisciplinaire **HAL**, est destinée au dépôt et à la diffusion de documents scientifiques de niveau recherche, publiés ou non, émanant des établissements d'enseignement et de recherche français ou étrangers, des laboratoires publics ou privés.

Ceres: Evolution and current state

Thomas B. McCord
Hawaii Institute of Geophysics and Planetology, University of Hawaii, Honolulu, Hawaii, USA

Christophe Sotin
Laboratory de Planetologie et Geodynamique, University of Nantes, Nantes, France

Received 30 January 2004; revised 20 January 2005; accepted 18 February 2005; published 21 May 2005.

[1] We modeled several thermal evolution scenarios for Ceres to explore the nature of large, wet protoplanets and to predict current-day evidence that might be found by close inspection, such as by the Dawn mission. The density for Ceres is near 2.1, suggesting a water content between 17% and 27% by mass. Short- and long-lived radioactive nuclide heating is considered. Even if only long-lived radionuclide heating is assumed, the water ice in Ceres melts quickly and a water mantle forms, but an approximately 10-km crust does not melt. The circulating warm water would alter the silicates. As heat is lost by conduction through the frozen crust, water begins to freeze out at the base of the crust. Solid-state convection begins and transports more heat as well as perhaps material dissolved or entrained in the water to or near the surface. Ceres' water layer eventually (but perhaps not entirely) freezes, forming a layered density structure with perhaps some liquid water remaining today. Our differentiated models are in agreement with the recently measured difference between the equatorial and polar radii. We find that Ceres' existence and evolution depend critically on it containing water at formation, and this depends strongly on the combination of when it accreted and the amount of ^{26}Al present in the pre-Ceres $\sim$1-km-sized objects; slightly more ^{26}Al or earlier accretion produces a dry Vesta-like object. Melting and freezing plus mineralization would lead to several dimensional changes over time, creating topographic features, zones of weakness, and perhaps disruptions in the crust.

Citation: McCord, T. B., and C. Sotin (2005), Ceres: Evolution and current state, *J. Geophys. Res.*, *110*, E05009, doi:10.1029/2004JE002244.

1. Background

[2] Ceres orbits the Sun and is large enough in size to have experienced many of the processes normally associated with planetary evolution. Therefore it should be called a planet. Its location, in the middle of the asteroid belt, has caused it to be referred to as an asteroid. However, its size, orbit and general nature, as best we can discern it, suggest that it is much more interesting than the small pieces of larger objects (perhaps such as Ceres) that one normally thinks of when one refers to asteroids. Ceres' planet-like nature and its survival from the earliest stages of solar system formation, when its sister/brother objects probably became the major building blocks of the Earth and the other terrestrial inner planets, makes it an extremely important object for understanding the early stages of the solar system as well as basic planetary processes.

[3] Ceres' history and its relevancy to the other terrestrial planets motivated NASA to select DAWN in December 2001, a mission to orbit Ceres and Vesta, as a Discovery Program mission to be flown. Thus, in this article we review current knowledge and then explore through modeling the possible nature of Ceres and hopefully set the baseline for its future exploration. We are especially interested in predicting the internal structure and the nature of the surface of Ceres: the features and materials likely to be found by DAWN. These results should help in planning the DAWN mission. The other main object for DAWN is Vesta, which is not treated here but which has been recently reviewed by *Keil* [2003].

2. Current Knowledge

[4] Ceres was discovered in January/February 1801 by Giuseppe Piazzi in Palermo, Italy, while looking for the planet predicted by the Titus-Bode law to be located at about 2.8 AU from the Sun [*Piazzi*, 1802; *Encyclopædia Britannica*, 2004]. This was while a German team, following on the German Titius-Bode prediction, was also searching for the Ceres object. These German scientists instead found Vesta. Thus it seems appropriate that German and Italian teams are major contributors to the DAWN mission. Several recent publications give useful summaries of the general knowledge of Ceres and discuss and improve on the knowledge of its principal characteristics [*Parker et al.*,

Copyright 2005 by the American Geophysical Union.
0148-0227/05/2004JE002244

Table 1. Mass of Ceres[a]

Reference	Method (Perturbations on)	Mass (Solar Mass)	Error	Mass, kg
Viateau and Rapaport [1998]	9 asteroids	4.759E − 10	0.023	9.47E + 20
Michalak [2000]	25 asteroids	4.700E − 10	0.04	9.35E + 20
Standish [2001]	Mars	4.762E − 10	0.015	9.47E + 20
Average		4.740E − 10	0.026	9.43E + 20

[a]Values for the mass of Ceres are given for the most recent and likely most accurate, as judged by the authors. A single value is determined by simply averaging, and this value is used in the modeling and analysis described in this article.

2002; *Britt et al.*, 2002]. We attempt, from the recent works available to us, to select the most likely correct values of these fundamental characteristics (Table 1), with which to conduct our discussion and modeling efforts. These values will certainly improve with time, but it seems that they are sufficiently known at this time to proceed with the modeling effort. Refinements certainly should be made before DAWN reaches Ceres in about 2014.

2.1. Orbit

[5] Ceres orbits the Sun at a mean heliocentric distance of a = 2.767 AU, has a proper eccentricity of e = 0.097 and an inclination of 9.73 degrees. The rotational period is given by *Lagerkvist and Magnusson* [1990] as 9.076 hours. The pole position has been difficult to pin down because of the small variations in its light curve but the spin pole is believed to be nearly perpendicular to the orbit plane. Thus it is a relatively easy object to reach from Earth.

2.2. Mass

[6] The mass of Ceres has been determined repeatedly with (hopefully) ever improving results. The traditional method is by measuring the perturbations of Ceres' mass on the orbits of other objects, e.g., asteroids and Mars, and the longer the orbital disturbances are observed the more accurate becomes the mass determinations. Thus we turn to the most recent calculations. *Michalak* [2000] determined a Ceres mass of $4.70 \pm 0.04 \times 10^{-10}$ solar masses from observing the gravitational perturbations on the orbits of 25 different asteroids. *Viateau and Rapaport* [1998] reported a mass of $4.759 \pm 0.023 \times 10^{-10}$ solar mass from the perturbations on the orbits of 9 asteroids. These are very similar results derived totally independently (M. Rapaport, personal communication, 2002) but by the same method. *Standish* [2001] reported his most recent Ceres mass calculation of $4.762 \pm 0.015 \times 10^{-10}$ solar masses in the process of maintaining and updating planetary ephemeredes in association with planning and executing spacecraft missions, following earlier analyses [*Standish and Hellings*, 1989]. These three values are used by us as the likely most accurate.

[7] However, *Hilton* [1999] reported a mass for Ceres of $4.39 \pm 0.04 \times 10^{-10}$ solar masses. This value is incompatible with the previous three values and many earlier determinations. There is apparently difficulty finding an explanation for this (M. Rapaport (personal communication, 2002) and discussed by *Hilton* [1999]). Thus there remains an uncertainty beyond the formal errors given in the three determinations used in Table 1. Further analysis of this uncertainty might use the earlier reported mass values, such as listed by *Britt et al.* [2002] and by *Schubert and Matson* [1979].

2.3. Size and Shape

[8] There have been three different methods of measuring the size and shape of Ceres: (1) occultation of a star by Ceres as seen from the Earth, (2) Earth-orbital Hubble Space Telescope camera direct imaging, and (3) adaptive optics (AO) imaging with ground-based telescopes. *Millis et al.* [1987] used multiple stellar occultation measurements to determine Ceres to be an oblate spheroid with an equatorial radius of 479.6 ± 2.4 km and polar radius of 453.4 ± 4.5 km. *Parker et al.* [2002] reported their most recent analysis of the Ceres images they obtained using the Hubble Space Telescope/Faint Object Camera. Ellipse fits were performed to each of the good signal HSWT images. These gave values of projected semimajor and semiminor axes of 484.8 ± 5.1 km and 466.4 ± 5.9 km. *Drummond et al.* [1998] used an adaptive optics imaging system on a 1.5-m ground-based telescope to obtain images of Ceres. A triaxial ellipsoid model for Ceres was derived from 17 images. The model dimensions depended somewhat on which solution of the pole position was selected from the two they derived. An average of these two possible models gives radii of 508 ± 5 km and 472.5 ± 6.5 km. This model was reported to be in "excellent agreement" with

Table 2. Shape of Ceres[a]

Reference	Method	RAD-1, km	Error, km	RAD-2, km	Error, km	Equatorial Radius, km	RAD-3 Polar, km	Error, km	Effective Radius, km
Millis et al. [1987]	occultation	479.6	2.4			479.6	453.4	4.5	471
Saint-Pe et al. [1993]	adaptive optics	499	20			(499)	469	20	(489)
Drummond et al. [1998]	adaptive optics	508	5	472.5	5	490	445.25	5	475
Parker et al. [2002]	HST obs	484.8	5.1			484.8	466.4	5.9	479
Average		493		472.5		485 (488)	455 (459)		475 (479)

[a]Values for the shape of Ceres are given for the most recent and likely most accurate, as judged by the authors. A single value for each radius is determined by simply averaging and a series of effective radii are calculated: $r_{eff} = (r_{eq}^2 \times r_{polar})^{1/3}$. The final result is a value of 475 km for the effective radius that is used in the modeling and analysis described in this article. The value in parentheses is the one obtained by taking into account the value of *Saint-Pe et al.* [1993], which is larger than the three other referenced values.

the occultation results and the earlier AO images by *Saint-Pe et al.* [1993], who gave values of 499 ± 20 km and 469 ± 20 km. These values are reported in Table 2. The effective radius (r_{eq}) of a sphere of volume equal to that of the measured ellipsoid is calculated (Table 2). The effective radius of *Saint-Pe et al.* [1993] is much larger than the three other measurements. Therefore we adopt a value of 475 km for our analysis as being most representative of the probable actual value.

2.4. Bulk Density

[9] Using the values in Tables 1 and 2, a density can be calculated. First, we have averaged the mass values to acquire our model number of 4.740×10^{-10} solar masses, with an estimated uncertainty of $0.026\ 10^{-10}$ solar masses. Using a solar mass of 1.989×10^{30} kg, leads to a Ceres mass of 9.43×10^{20} kg with an estimated uncertainty of 0.05×10^{20} kg or about 0.5%. From the several ellipsoid models of the shape of Ceres given in Table 2, a series of effective radii are calculated: $r_{eff} = (r_1 \times r_2)^{1/2}$. This leads to a formal model radius value of 475.04 km or a diameter of 950.08 km, with an estimated uncertainty of order 10 km in radius, or about 2%. This gives a volume for Ceres of $4/3\ \pi\ r^3 = 4.49 \times 10^8$ km^3 or 4.49×10^{23} cm^3. The resulting bulk density is mass/volume = 9.43×10^{23} gm/4.49×10^{33} cm^3 = 2.10 gm/cc.

[10] Many small solar system objects are known to be underdense; i.e., they are unconsolidated and have large porosity [cf. *Britt and Consolmagno*, 2000]. *Thomas et al.* [1986] showed that small objects tend to be irregular in shape but that at a size much smaller than Ceres (>10^7 km^3) the shape becomes near spherical suggesting that their gravity is sufficient to compress the material and eliminate pore spaces. *Britt et al.* [2002] review this topic, and *Johnson and Anderson* [2003] elaborated on this point in their study of Amalthea. Thus we believe that Ceres' density is an accurate indication of the density of the composite materials and that its porosity is very low below its regolith.

[11] From bulk density can be drawn some inferences about the general composition of an object. Comparing the density of Ceres with those of other small planet-sized objects (Table 3) shows that Ceres is similar to the two outer Galilean satellites, Ganymede and Callisto. The magnetic [*Kivelson et al.*, 2002] and radio-science gravity data [*Anderson et al.*, 1996] returned by the Galileo mission show that Ganymede has undergone differentiation processes that lead to the formation of an liquid iron core, silicate mantle and outer H_2O layer. Callisto is less differentiated [*Anderson et al.*, 1998a] but still has large amounts of liquid water [*Kivelson et al.*, 1999]. These two objects are less evolved than the inner Galilean satellites Europa and certainly Io, and are thought to contain considerably larger amounts of water. Vesta is considerably more dense and is known to be highly thermally evolved [*McCord et al.*, 1970; cf. *Keil*, 2002], as of course is the Moon. Pallas is also denser than Ceres, but the reason (thermal evolution or low water at birth) presently is unclear. Titan is less dense, but knowledge of its composition and structure is poor [cf. *Grasset and Sotin*, 2000]. Thus Ceres seems wetter and less evolved, more like Callisto or Ganymede, than Vesta or Europa.

Table 3. Comparison of Total Object Densities[a]

Object	Density
Vesta	3.44
Moon	3.34
Europa	2.97
Pallas	2.71
Ceres	*2.10*
Ganymede	1.94
Titan	1.88
Callisto	1.86

[a]The density of Ceres is shown compared with density values for some other small planet-like objects. The density of Vesta is from the mass by *Standish* [2001] and the volume from *Thomas et al.* [1997], following discussions by *Keil* [2002] and *Britt et al.* [2002].

2.5. Albedo

[12] *Millis et al.* [1987] reported a V(λ = 5600 A) geometric albedo of 0.073. *Parker et al.* [2002] calculated geometric albedos of 0.056 near-UV (λ = 3636A), 0.029 mid-UV (λ = 2795A), and 0.090 far-UV (λ = 1621A). *Tedesco* [1989] gives a visual albedo of ~0.10. Interestingly, all these values are well above the albedo of carbonaceous chondrite (Cc) material [*Johnson and Fanale*, 1973], which is in the range of 3 to 5%. Thus there must be brighter material mixed with the Cc material if Cc material is present. As we will show below, altered Cc material, generated in the interior thermal evolution of Ceres, such as salts with high albedos, could reach the surface. This high albedo is consistent with that result.

2.6. Temperature

[13] All observations of Ceres so far made are of a nearly fully Sun illuminated hemisphere, given the relative orbital characteristics of the Earth and Ceres. Further, they are of the integral hemisphere and so average over longitude and latitude variations in illumination as well as local variations in material and albedo. These will be the highest temperatures for the entire surface.

[14] *Dotto et al.* [2000] presented an analysis of the ISO 5.8–11.6-μm spectral results for Ceres. STM subsolar temperatures of 215 K were calculated using the Standard Thermal Model (STM) [cf. *Lebofsky and Spencer*, 1989]. They then modeled the observed ISO fluxes using an advanced Thermo-Physical Model (TPM) and achieved a good fit, suggesting that the temperatures were realistic. *Deutsch et al.* [1997] analyzed MIRAC2 images of Ceres taken between 8.6 and 20.6 μm. Ceres was resolved at all wavelengths except 20.6 μm. The measured fluxes at these wavelengths were well fitted by a 238 K blackbody flux model. In addition, they found variations over the surface of Ceres of the opacity/emissivity. *King et al.* [1992] used the STM to calculate an effective surface temperature for the integral disk of Ceres of 231.5 K.

[15] *Fanale and Salvail* [1989] calculated a near subsurface temperature (below diurnal variations but due to insolation) as a function of latitude to range from 180 K at the equator to near 130 K at the poles. This is for an albedo of 0.09, circular orbit and zero spin-pole obliquity. This was done in support of their calculations to determine the stability of water ice below the surface. One might assume that there are variations of albedo and therefore temperature over the surface. This is of interest in determining the stability of materials and interpreting flux

observations at particular locations on the surface. However, the Fanale and Salvail calculation is of more interest for models of the subsurface behavior.

2.7. Spectral Reflectance

[16] The spectral reflectance of Ceres over the range where solar radiation is significant has been measured in bits and pieces and with increasing precision over time. The approach is to determine the surface minerals and molecules by identifying absorptions in the reflectance spectrum. The reflectance of Ceres became usefully defined for interpreting surface mineralogy when electronic detectors on large telescopes became available and IR observations possible. *Chapman et al.* [1973] first reported on modern observations of Ceres and other asteroid and showed the Ceres spectrum in the 0.4 to 1.0-μm range to be flat and featureless except for a strong decrease in reflectance shortward of about 0.45 μm. A summary of these early observations in the visible and near IR spectral range is given by *Gaffey and McCord* [1978]. The spectral range observed was extended into the infrared from 1.0 to 2.6 μm by *Larson et al.* [1979]. They showed a slightly rising reflectance toward the longer wavelengths but with no discernable absorption features. This suggested no extensive water on the surface because the 1.9-μm-water absorption feature was absent.

[17] Attempts were made to interpret these early measurements in this spectral range in terms of meteorite and other mineral compositions. *Chapman and Salisbury* [1973] and *Johnson and Fanale* [1973] found no match to Ceres among available meteorite or other mineral spectra. The latter authors, however, did create a carbonaceous chondrite-like laboratory mix of carbon black, montmorillonite and hydrated silicate minerals and were able to mimic the Ceres spectrum. *McCord and Gaffey* [1974] similarly proposed an opaque-rich assemblage probably like carbonaceous material. However, even though the Ceres spectrum in the visible and near IR had become associated with Cc-type meteorites, interpretations were offered ranging from primitive carbon-rich hydrous silicate mixtures (C1) to metamorphosed mafic silicates and iron oxides (C4) [e.g., *Gaffey and McCord*, 1978; *Chapman*, 1975, 1976].

[18] Of great interest was the first report of a 3-μm absorption in the spectrum of Ceres interpreted to be due to OH and perhaps H_2O [*Lebofsky*, 1978, 1980]. This clearly identified the Ceres surface material with aqueous altered material such as clays and hydrated salts similar to CI and CM, i.e., primitive, Cc meteorites. *Lebofsky et al.* [1981] presented further observations of Ceres in the 1.7–4.2-μm range. They confirmed and elaborated on the 3-μm absorption and concluded that the strong absorption at 2.7–2.8 μm is due to structural OH groups in clay minerals. They reported that the dominant minerals on the surface of Ceres are therefore hydrated clay minerals structurally similar to terrestrial montmorillonites. They also reported a narrow absorption feature at 3.1 μm and interpreted it as being due to a very small amount of water ice on Ceres, making this the first evidence suggested for ice on the surface of an asteroid.

[19] *Feierberg et al.* [1981] re-presented the then-recent observational data for Ceres and compared these with laboratory measurements of some hydrated materials. They concluded that the 3-μm feature is largely due to interlayer water molecules in clay minerals with a possible contribution from water molecules bound to salts. They reported that Ceres must consist mostly of clay mineral like that in CM chondrites with some contributions to the strength of the 3-μm band by hydrated salts. They point out that the salts are products of aqueous alteration and may also be responsible for Ceres' high albedo relative to other C-type asteroids. They comment further that the spectra of C-type asteroids in general may be reconcilable with those of carbonaceous chondrites if the asteroids' surfaces have undergone alteration by aqueous or other analogous processes [cf. *Jones et al.*, 1988, 1990].

[20] A decade later, *King et al.* [1992] reported new observations of Ceres in the 3-μm region and confirmed the narrow absorption near 3.1 μm, reported by *Lebofsky et al.* [1981]. They, however, concluded by comparisons with the USGS spectral library that the feature could not be due to OH, H_2O, CO_3, SO_4 or other ions containing oxygen in geological materials. Further, they felt that the feature is too narrow and at too long a wavelength to be due to water ice from theoretical calculations of ice spectra, although the laboratory data for frosts by *Lebofsky et al.* [1981] appear to fit better than the calculated spectra. Instead, they attributed the feature to HN_4-bearing minerals including naturally occurring buddingtonite and other minerals. They found the Ceres absorption to be most similar to an NH_4-bearing saponite, which is a trioctahedral smectite that commonly forms from hydrothermal alteration or weathering of basic rocks and, they pointed out, has been reported in aqueous alteration products in CV and CI carbonaceous chondrites and may be present in CM carbonaceous chondrites. They interpret the apparent presence of ammonium-bearing mineral species to suggest that the secondary temperature for this Ceres material could not have exceeded 400 K from the thermal stability of these materials.

2.8. UV Emission

[21] A somewhat startling observation was reported using the International Ultraviolet Explorer (IUE) satellite in Earth orbit to observe Ceres [*A'Hearn and Feldman*, 1992]. Spectroscopic observations were interpreted to suggest an emission at 3080 A associated with the northern limb of Ceres. They pointed out that this is consistent with the emission feature due to the O-O band of OH molecule, which is usually seen in cometary spectra. Since H_2O is difficult to detect and readily photodissociates in sunlight, it is not known whether it is also present or is the source molecule. They calculate a possible production of H_2O from Ceres in the range of 10^{24} to 10^{25} sec^{-1} to explain the observations. They point out that this is consistent with the estimates of *Fanale and Salvail* [1989] for a flux that could be sustained over geologic time from subsurface ice layer supplied from below.

3. Models of Ceres Evolution

3.1. Background and Assumptions

[22] From the spectral reflectance, the low density and the location in the Solar System, it is thought that Ceres was formed mostly of unaltered carbonaceous chondrite source material with water ice. Evidence from these and other meteorite types suggests that Ceres and other asteroids

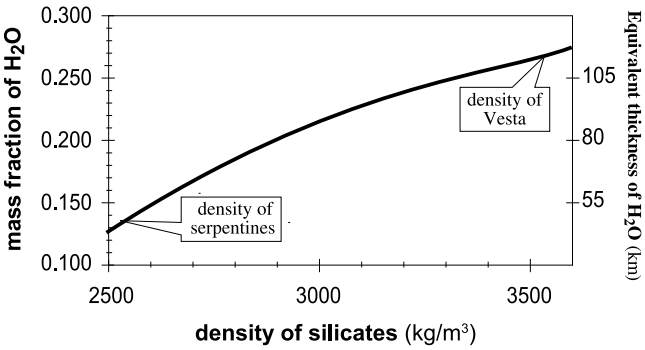

Figure 1. Mass fraction of H_2O as a function of the density of the core. The right scale is the thickness of the outer H_2O layer in a model where H_2O and silicates are fully differentiated.

formed very early in the age of the Solar System, probably within a few up to about 10 million years. Ceres' size and orbit suggest that it has not been fragmented and remains approximately the size and location from formation. Ceres' low density (Table 3) indicates that considerable water is currently present, as does the association of the surface material with altered Cc meteorite types and the presence of OH and perhaps H_2O. If one assumes a simple mixture of water (density of 1) and silicate rock with density between that of serpentine (2.54) [*Christensen*, 1978] and Vesta (3.44), Ceres currently could be between approximately 17% and 27% water by mass (Figure 1). The silicate and water ice mass proportions in the material available for forming bodies like Ceres early in the history of the solar system is thought to be something like 75% and 25%, respectively [cf. *Wilson et al.*, 1999; *Grimm and McSween*, 1989]. This suggests that most of the water present at formation remains in some form within Ceres.

[23] The thermal evolution of carbonaceous chondrite parent bodies has been studied previously. *Grimm and McSween* [1989] presented the first quantitative models, following qualitative discussions by *DuFresne and Anders* [1962]. (See *McSween et al.* [2002] for a recent review and update.) Their motivation was to explore how the aqueous alterations seen in Cc meteorites could occur in the parent bodies early in their histories. They pointed out the important role of water ice in the interior of a thermally evolving Cc parent body in moderating the temperature gradients so as to prefer low temperature alteration such as seen in Cc meteorites. Water ice must absorb large amounts of heat energy by melting (latent heat of fusion) and the resulting warm liquid water must also distribute heat within the body by convection.

[24] *Grimm and McSween* [1989] and *McSween et al.* [2002] presented in-depth discussions of the initial conditions used for their models, many of which we use as the basis for our models. *Grimm and McSween* [1989] considered an initial body with a cold mix of silicates and ice. The heat source was assumed to be the decay of ^{26}Al to ^{26}Mg, evidence of which is found today in calcium-aluminum-rich inclusions (CAIs) [cf. *MacPherson et al.*, 1995]. They then explored evolution scenarios by varying the object diameter, water volume fraction and initial ^{26}Al/^{27}Al ratio. Although they presented results for bodies up to 1000 km in diameter, about the same as Ceres, they restricted their focus to smaller bodies and early low-temperature aqueous alterations to help explain evidence seen in the Cc meteorites, and they did not include thermal effects of mineral alteration (except for melting of ice) and degassing.

[25] Although we follow essentially the same path, we focused on the larger object, Ceres, extend our consideration throughout the age of Ceres using long-lived radionuclide heat sources as well as ^{26}Al, considered energy effects of mineralization, all to suggest the plausible materials and conditions on and in Ceres today.

[26] It is generally accepted that carbonaceous chondrite meteorite material was aqueously altered from its source material (ice and silicates) at warm but still low temperatures in the parent bodies and then was brecciated very early in the history of the solar system [cf. *Krot et al.*, 2003]. The temperature was apparently within ~50 deg. of the melting temperature of water ice during aqueous alteration, suggested by oxygen-isotopic partitioning in CM and CI chondrites [*Clayton and Mayeda*, 1984, 1999; *Leshin et al.*, 1997; *Young et al.*, 1999]. It is thought likely that brecciation and alteration to CM meteorite material occurred within a few million years of chondrule and CAI formation, about 4.5 by ago [*Swindle et al.*, 1988; *Allegre et al.*, 1995; *Krot et al.*, 1999] and was driven by decay of ^{26}Al. We assume that Ceres evolved in a similar way to the parent bodies of the Cc meteorites at first but, being larger and spared catastrophic breakup [e.g., *Greenberg and Chapman*, 1983], Ceres evolved further. We focus on Ceres and not on the much smaller Cc meteorite parent bodies. They both may have formed from the same basic materials, but the aqueous thermal evolution in the large bodies probably was different: higher temperatures, longer periods of heating, differentiation.

[27] A large uncertainty in modeling the early thermal evolution is the amount and kind of short-lived radioisotopes incorporated into a forming Ceres. *Grimm and McSween* [1989] considered only ^{26}Al as a short-lived

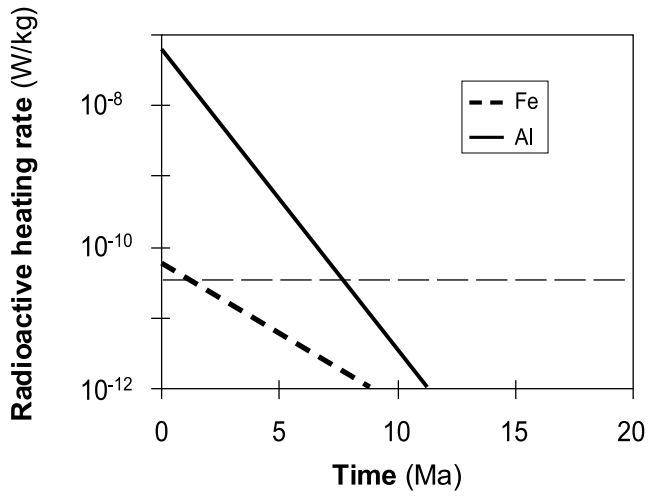

Figure 2. Comparison of the heat produced by ^{26}Al, ^{60}Fe (the next strongest contributor), and long-lived (horizontal line) radioactive elements. Initial time may be seen as the time of formation of CAIs.

Table 4. Quantities Used to Compute Temperature Profiles[a]

	Silicate	Ice	Mixture of Ice and Silicates
Density (ρ)	2.54 to 3.44[b]	1.0	$fs.\rho_S + (1\text{-}fs).\rho_I$
Thermal conductivity (k in W/m/K)	4.2	0.4685 + 488.12/T	$fs.k_S + (1\text{-}fs).k_I$
Heat capacity (C in J/kg/K)	920	185 + 7.037 T	$xs.C_S + (1\text{-}xs).C_I$
Thermal expansion, K^{-1}	$2.4\ 10^{-5}$	$2.5\ 10^{-7}.T - 1.25\ 10^{-5}$	Not necessary

[a]The parameters xs and fs are mass fraction and volume fraction of silicates, respectively. Subscripts S and I correspond to silicates and ice, respectively. T is temperature in Kelvin.

[b]A density of 3.44 is the density of Vesta, which is supposed to be free of H_2O. Such a value is close to the density of the Earth's upper mantle.

source and in amounts from 1 to 6×10^{-6} parts per ^{27}Al. We use the same assumption, but we also carry our calculations to longer times and use long-lived radionuclides U^{238}, Th^{232} and K^{40} in their abundance found in Cc meteorites [*Mason*, 1971]. The reason for considering only ^{26}Al of the potential short-lived radionuclides can be seen in Figure 2. The other candidates have half-lives too short and probably occurred in quantities too small to contribute significantly compared to ^{26}Al and the long-lived sources of energy to Ceres' evolution.

3.2. Model

[28] We use a finite difference spherically-symmetric code to determine the thermal evolution of Ceres. This is a modified version of the model used to explore the evolution of Europa's core [*Tobie et al.*, 2003]. The one dimensional conservation of energy equation can be written [e.g., *Turcotte and Schubert*, 1981]:

$$\frac{\partial\left(k.^{\partial T}/_{dr}\right)}{\partial r} + \frac{2}{r}\left(k\frac{\partial T}{\partial r}\right) = \rho C_P\left(\frac{dT}{dt}\right) - H_R,$$

where values of thermal conductivity (k), volumetric radiogenic heating (H_R), density (ρ) and heat capacity (C_P) depend on the fraction of ice. Values of the different parameters are given in Table 4, and the radiogenic heating parameters used are given in Table 5. The boundary conditions are prescribed temperature at the surface and zero temperature gradient in the center (dT/dr = 0). The initial temperature profile is set to a constant temperature, which is the prescribed surface temperature.

[29] In our calculations, we assume that the density of H_2O is equal to 1.0 whatever the phase (liquid or solid). The density of silicates varies between that of serpentines (2.54) [*Christensen*, 1978] and that of Vesta (3.44 [*Britt et al.*, 2002]), which is supposed to contain a negligible amount of volatiles.

[30] Vesta is the reference for calculating the amount of radiogenic elements. The amount of each radiogenic element (m_R) is given by $m_R = C_R M_{sil}$ where C_R is the concentration of the radiogenic element per kg of silicate and M_{sil} is the mass of silicates. However, the mass of silicates depends on the density we choose for the silicates (Figure 1). The larger the density of silicates is, the smaller the total mass of silicates must be because the mass of Ceres is known and fixed in this calculation. The mass of silicates is given by

$$M_{sil} = \frac{\rho_{sil}}{\rho}\frac{(\rho - \rho_w)}{(\rho_{sil} - \rho_w)}M_{Ceres},$$

where ρ is the density of Ceres and ρ_w the density of H_2O. Therefore we use the density of Vesta to determine the total mass of radiogenic elements. Then we divide the total mass of radiogenic elements by the volume of silicates to get the volumetric radiogenic heating rate, which is the quantity required in the heat conservation equation. All constants in the model depend on the mass fraction of silicates and ice.

[31] The present models assume instantaneous cold accretion of Ceres from ~1-km-sized objects that themselves earlier accreted from solar nebula during a duration period ~2.4 Myr from nebula cooling and formation of CAIs. Models of the formation of Ceres-sized objects accreting from kilometer-sized planetesimals suggest accretion time in less than 0.1 Myr [*Weidenschilling et al.*, 1997]. This accretion time seems short enough to have no significant thermal effect, as is discussed in section 3.5. The only heat sources assumed in our Ceres evolution calculations are radionuclides U^{238}, U^{235}, Th^{232} and K^{40} (long-lived) and the remaining ^{26}Al (short-lived). We used as a baseline the generally accepted $^{26}Al/^{27}Al$ ratio of 5×10^{-5} at the time CAIs formed [*Lee et al.*, 1976; *Srinivasan et al.*, 1999]. Because the duration time, i.e., the time between the formation of CAIs and the beginning of Ceres' accretion from kilometer-sized objects, is not well constrained [*Canup*, 2004], we have investigated different concentrations of $^{26}Al/^{27}Al$, and the results are discussed in section 3.5.

[32] The heating caused by the decay of ^{26}Al during the accretion of small H_2O-free asteroids has been investigated previously [*Merk et al.*, 2002; *Ghosh et al.*, 2003]. If accretion was completed in less than 5 Myr, the amount of heat released by the decay of ^{26}Al is several orders of magnitude larger than that due to the long-lived radiogenic

Table 5. Radiogenic Heating Parameters Used in the Models[a]

Element	C_0, ppb	H_0 (mW/kg of Element)	Half-Life, Myr
^{26}Al	450	138	0.716
^{60}Fe	0.8	74.7	1.5
^{40}K	430	0.0619	1250
^{232}Th	130	0.0204	14000
^{235}U	17.5	0.401	704
^{238}U	52.4	0.104	4470

[a]The volumetric radiogenic heating rate is given by $H_R = \rho x_S \sum_{i=1}^{n} C_0 H_{0,i} e^{-\lambda_i t}$, where ρ is the density of the mixture of ice and rock, xs is the mass fraction of silicates, n is the number of radiogenic elements (n = 6), and $H_{0,i}$ is the initial power of radiogenic decay per unit mass of radiogenic element i with decay constant λ_i. The initial time (t_0) is that of the formation of CAIs (see text). This table also gives the initial concentration of radiogenic elements (C_0). These values are discussed in the text.

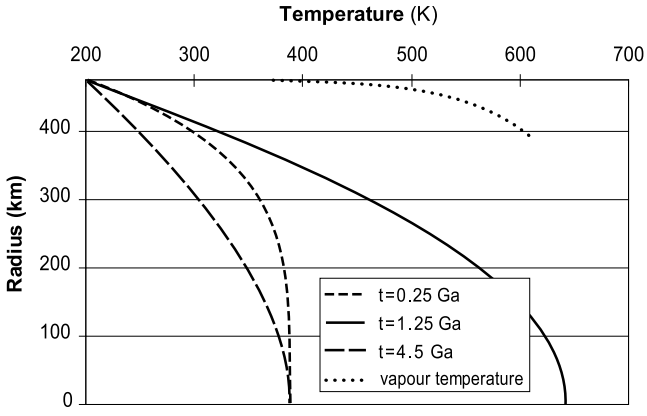

Figure 3. Temperature profiles versus radius at different times. The dotted curve is the vaporization curve, which is drawn to show that vapor cannot form in the deep interior of a big asteroid. The three temperature profiles illustrate key steps described in the text.

elements at that time (Figure 2) and caused melting inside the body [*Merk et al.*, 2002]. The present study extends these models for larger objects having a significant amount of water ice. The thermal diffusive time for a kilometer-sized object is $t \sim d^2/K = 10^{12}$ sec = 30,000 years. Thus the object cools rapidly because heat is dissipated very efficiently. Therefore we ran models with different values of $^{26}Al/^{27}Al$ and for different model starting times relative to ^{26}Al half-life, which is effectively the same thing, to explore the effects. However, we discuss here only models that start with water ice still present; i.e., we do not discuss here models that start early enough (short duration time) and with enough ^{26}Al remaining to remove all water from the model object, since Ceres probably contains a large amount of water, given its bulk density of about 2.1.

[33] When the temperature becomes larger than the melting temperature of ice, latent heat of ice must be considered, as described in evolution scenario 1 (section 3.3). During melting, temperature is held constant until enough energy has been accumulated to melt the ice. Then silicates differentiate from water. A second evolution scenario (section 3.4) takes into account the differentiation of the mixture of ice and silicates upon melting of ice and the cooling and freezing of the H_2O layer, which also may undergo convective processes. Then, in section 3.5, we discuss the effects of aqueous alteration of the silicates, and the different assumptions including duration time, instantaneous accretion, surface temperatures, and ^{26}Al amount.

3.3. Description of Evolution Scenario 1 (No Differentiation)

[34] We begin with a model object that is a homogeneous mixture of ice and silicate grains that has an initial temperature of 200 K, and is made of a mixture of 74% mass fraction of silicates (density 3.44) and 26% mass fraction of ice (density 1.0). We neglect any temperature increase due to accretion and we assume the initial temperature profile is isothermal.

[35] We assume rapid accretion of the Ceres object occurs from smaller (<1 km) unmelted bodies immediately after these small bodies formed, selecting a time of 2.4 Myr after the formation of CAIs, following discussion by *Srinivasan et al.* [1999]. This allows the remaining ^{26}Al to decay and produce heat within the Ceres model object from 2.4 Myr after CAIs. This remaining amount of ^{26}Al at that time, assuming $5 \times 10^{-5} = {}^{26}Al/{}^{27}Al$ at CAIs and a half-life of 0.716 Myr, is about 10 times less than at CAIs (Figure 2).

[36] In less than 5 Myr, the Ceres center temperature becomes greater than the melting temperature of ice (273 K). The latent heat of ice melting is taken into account and during the next 10 Myr, the temperature profile is controlled by the melting of ice. Although different processes are likely to occur due to the presence of water (such as heat transfer by water circulation, differentiation into a rocky core and an outer liquid layer, alteration of silicates), these processes are first neglected in order to make this model as simple as possible. Heat is transferred only by conduction. In this simple model, the internal temperature continues to increase until the radiogenic heating rate becomes smaller than the heat that can be removed by conduction (t = 1.25 Ga, Figure 3) through the crust. Then, the body starts

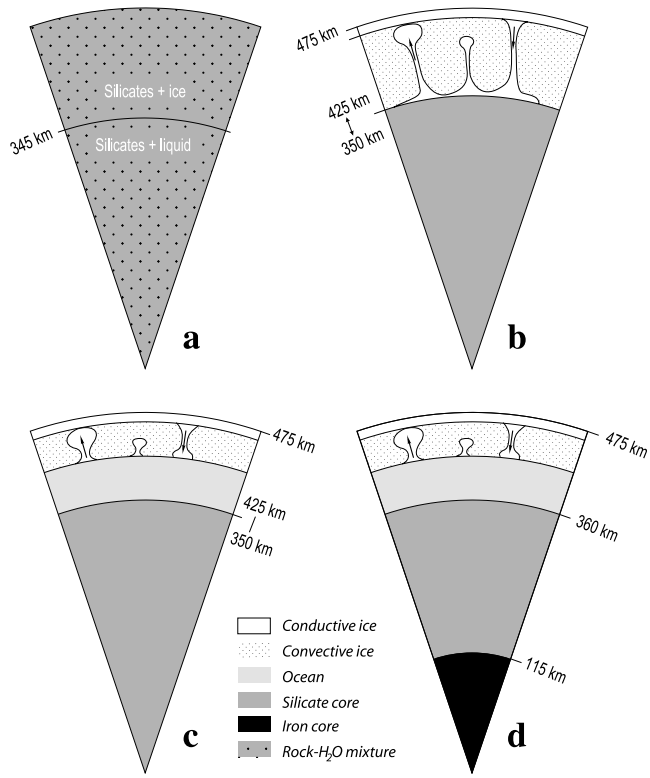

Figure 4. Different internal structures based on different scenarios described in the text: (a) homogeneous asteroid made of a mixture of H_2O and high-density silicates, (b) differentiated Ceres with high-density silicate core equivalent to Vesta (core radius of 350 km) or low-density serpentine (core radius of 425 km) and outer ice layer, (c) same as Figure 4b but the presence of antifreezing material (ammonia) maintains a liquid layer, and (d) fully differentiated model of Ceres with an inner iron core. The moments of inertia for these different models are given in Table 6.

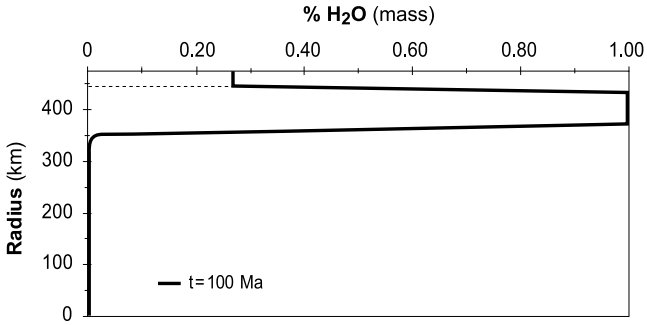

Figure 5. Amount of ice after 100 Myr. Internal temperatures are high, and ice melts and migrates to form an internal ocean. The outer layer does not reach temperatures high enough to allow for separation between silicates and ice. However, one might expect that compositional instability may reduce that thickness of the outer ice-silicate layer.

cooling down and the predicted internal temperature today is near 350 K, well above the ice melting temperature.

[37] In this model (no differentiation), Ceres would have liquid water in its interior today. The transition between ice-silicate material and liquid water embedded in a silicate matrix today would be 130 km deep (Figure 4a). This model resembles that of Callisto described by *Nagel et al.* [2004] except that Callisto being less dense (its uncompressed density is around 1.5) has an homogeneous rock-ice core covered by an H_2O layer.

[38] We ignored accretional energy input, but accretion of at least the last or top layers will increase their temperature. Assuming that all kinetic energy is transformed into temperature increase of the accreted material gives a maximum increase (once the body has reached its final radius) of 30K. Transformation of 50% of kinetic energy is more realistic. This temperature increase is small enough not to be taken into account, given the other uncertainties.

[39] Note that the water vaporization temperature is never reached in the interior (Figure 3) and so water vapor is not produced and water cannot escape. This result depends partly on our assumption [*Thomas et al.*, 1986; *Britt et al.*, 2002; *Johnson and Anderson*, 2003] that the porosity of the Ceres model object is small and the interior pressure being greater than the vacuum of space. At the surface, ice would sublime, but a silicate layer/regolith would form and ice could remain today within tens to hundreds of meters from the surface [*Fanale and Salvail*, 1989].

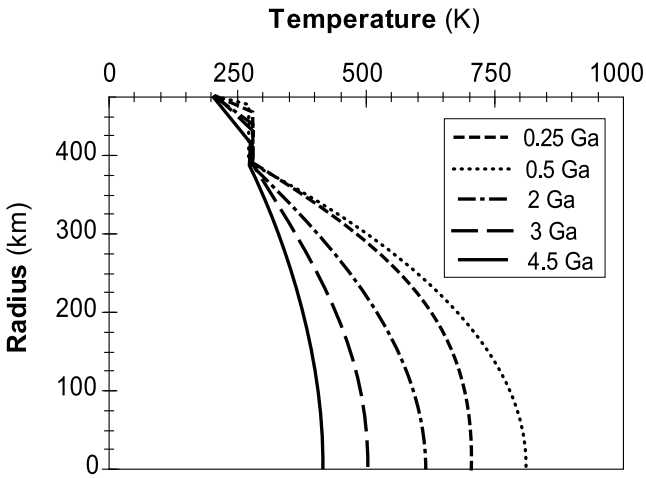

Figure 6. Temperature profiles in the case of a differentiated Ceres (model b in Figure 4).

3.4. Description of Evolution Scenario 2 (Differentiation)

[40] Due to the large amount of water in Ceres today, one may expect models resembling those for the large icy moons Europa or Ganymede [*Anderson et al.*, 1996; *Anderson et al.*, 1998a, 1998b]. On the basis of the value of the moment of inertia (MoI), these satellites are composed of a dense silicate core and an outer H_2O layer. Even an inner iron-rich core is predicted in order to explain Ganymede's magnetic field. Such a differentiated structure suggests that the water segregates from the silicates when the temperature exceeds the ice melting temperature. As described before, this event would occur in Ceres very quickly on geological timescales, about 10 Myr after accretion is completed. We therefore start evolution scenario 2 with an inner core (density 3.44) and an outer liquid H_2O layer about 100 km thick (Figure 5). It is however predicted that the outer layer of original mixed ice and rock does not melt to the surface because the surface temperature never reaches the melting temperature of ice (Figure 5) due to the high conductivity of the surface layer.

[41] Thermal evolution (Figure 6) is controlled by the H_2O layer. This layer cools from above leading to a three layers structure (Figure 5): the top 10 km is made of the original ice and silicates mixture, then a liquid mantle, and finally a silicate core. As described in Figure 7, as the heat flux decreases, the ice layer thickens. The thickness of the ice layer is controlled by the heat flux, which comes from the silicate core (Figure 8). A maximum value of the heat-flux (15 mW/m^2) exists at t = 1.2 Ga (Figure 8) and the thickness of the surface layer at that time would be about 20 km (Figure 7).

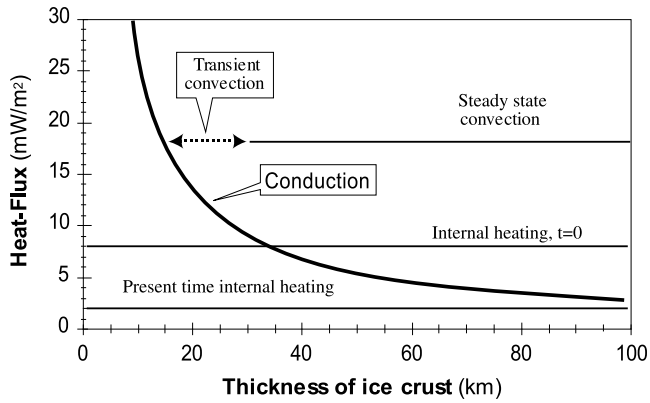

Figure 7. Heat flux versus thickness of the ice crust. Subsolidus convection (18 mW/m^2) becomes more efficient than conduction for a thickness larger than 20 km. The two horizontal lines represent equilibrium between heat flux and radiogenic heat production at present time and just after accretion.

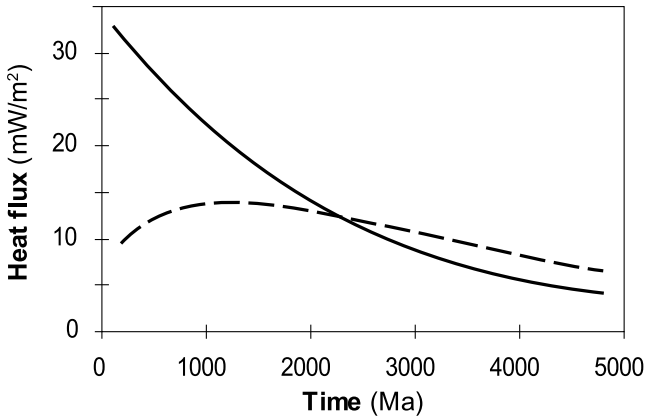

Figure 8. Heat flux versus time at the surface of the silicate core (dashed curve). The solid curve is the amount of radiogenic heating divided by the surface of the silicate core versus time (equilibrium heat flux). When this curve lies above the dashed curve, the core heats up. This explains why the maximum heat flux occurs around 1.2 Ga.

[42] One aspect of this thermal evolution scenario is the possibility of subsolidus convection in the ice layer above the liquid mantle. Convection models, which take into account the very strong temperature dependence of ice viscosity, can be built using scaling laws developed for icy satellites [*Sotin et al.*, 1997; *Deschamps and Sotin*, 2001]. Convection is predicted even though the gravitational acceleration is about five times smaller for Ceres. The different steps of the model are summarized here. The top and bottom boundaries of the ice layer are isothermal surfaces. The surface temperature is set to 200 K. The temperature at the interface between the ice crust and the liquid layer is the ice melting temperature of 273 K (due to the small pressure increase, the decrease of melting temperature with pressure for ice is not taken into account). Because ice viscosity depends very strongly upon temperature, convection processes are in the so-called conductive lid regime [*Solomatov*, 1995]: an outer conductive ice layer overlays a convective ice layer. The convective layer is bounded by two thermal boundary layers (TBL) where convective instabilities form. Numerical simulations [*Deschamps and Sotin*, 2001] and laboratory experiments [*Manga and Weeraratne*, 1999] suggest that the amount of heat that can be transferred by subsolidus convection is driven by the instabilities that form in the lower (hot) thermal boundary layer. Once stationary convection is reached, the thermal boundary layer is characterized by a constant value of the thermal boundary layer Rayleigh number (Ra_{TBL}):

$$Ra_{TBL} = \frac{\alpha\rho g(T_m - T_{ice})\delta^3}{\kappa\mu},$$

where δ is the thickness of the thermal boundary layer, α is coefficient of thermal expansion, μ is ice viscosity, κ is thermal diffusivity, and T_{ice} is temperature of the convective ice layer, which is the layer located between the two thermal boundary layers. The temperature difference ($T_m - T_{ice}$) across the thermal boundary layer is proportional to a viscous temperature scale ($\Delta T\mu$) [*Deschamps and Sotin*, 2001]:

$$T_m - T_{ice} = 1.43\Delta T_\mu = 1.43\left(\frac{-1}{\left(\partial Ln(\mu)/\partial T\right)_{T=Tice}}\right).$$

If one knows how ice viscosity depends on temperature, then one can calculate the temperature difference across the thermal boundary layer. Heat-flux can be calculated using conduction across the lower TBL:

$$q = \frac{Q}{4\pi R_m^2} = k\left(\frac{T_m - T_{ice}}{\delta}\right),$$

where δ is the TBL thickness determined by the third equation above, and R_m is the radius of the liquid-ice interface.

[43] Viscosity of ice is the key parameter controlling the amount of heat that can be transferred by subsolidus convection. Using a viscosity of 10^{14} Pa.s [*Sotin and Tobie*, 2004] and constants for ice reported in Table 4, the heat that can be transferred by convection is about 17 mW/m^2 (Figure 7) and convection could exist as soon as the thickness is larger than about 20 km. Such an event occurs late in the model developed for Ceres (1.5 Gyr after accretion) compared to the case for the large icy satellites [*Sotin et al.*, 1997]. With a surface temperature of 200 K, the model predicts a minimum conductive lid thickness on the order of 11 km. The thickness of the convective ice shell increases very quickly because the difference is large between the heat that can be removed by subsolidus convection in the ice and the heat flow at the silicate core/water boundary and the "ocean" freezes out. Taking a latent heat of 334 kJ/kg, we find that it takes between 200 and 400 Myr to freeze the liquid layer. Then global cooling of the body will slow down the convection process leading to three-layer structure: conductive lid, convective ice, silicate core (Figure 4b).

[44] Several processes can modify this model. The most important may be the presence of antifreeze material in the ice. As has been described in previous studies [e.g., *Sotin et al.*, 1997], the presence of ammonia decreases the melting temperature by about 100 K. Salt minerals are likely to be present and these also reduce the melting temperature of water. In that case, the present structure would be a four-layer structure (Figure 4c) with liquid water present today.

3.5. Discussion

3.5.1. Serpentinization

[45] As the warm water differentiates, it will react with the peridotite-like silicates. Olivine and pyroxene can transform into serpentine (lizardite or chrysotile $Mg_3Si_2O_5(OH)_4$) and brucite ($Mg,Fe(OH)_2$). Often, magnetite (Fe_3O_4) forms at the expense of iron-bearing brucite. An example of the reaction (assuming a Mg number of 20%) can be

$$2(Fe_{0.2},Mg_{0.8})_2SiO_4 + 3\ H_2O = Mg_3Si_2O_5(OH)_4 + (Mg_{0.2},Fe_{0.8})(OH)_2 = Mg_3Si_2O_5(OH)_4 + 0.2Mg(OH)_2 + 0.8/3\ Fe_3O_4 + 1.6/3\ H_2O + 0.8/3\ H_2.$$

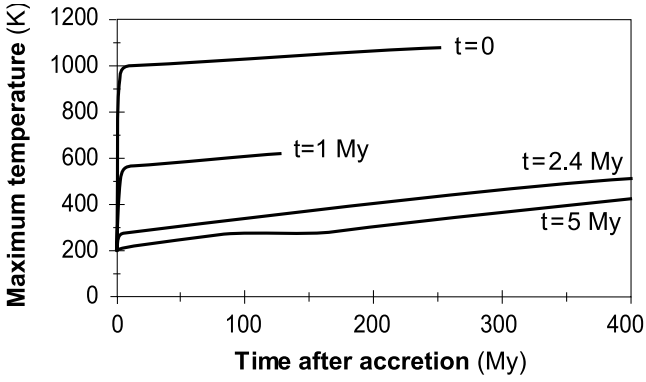

Figure 9. Maximum temperature (center of the small body) versus time for different times at which the planetesimals form. All models start with a 200 K temperature in the center. For t = 5 Myr, the plateau corresponds to the transformation of ice into water in the asteroid. For t = 2.4 Myr, this plateau exists almost at the beginning of the thermal evolution. For shorter times, the decay of ^{26}Al produces a very strong increase of temperature until all ^{26}Al disappears. Then, the heating is due to the decay of the long-lived radiogenic elements. The very high temperature makes unlikely this kind of model for Ceres since the water would vaporize and escape the accreting body.

[46] In this case the global reaction is

$$2 \text{ olivine} + 7.4/3\ H_2O = 1 \text{ chrysotile} + 0.2 \text{ brucite} + 0.8/3\ Fe_3O_4 + 0.8/3\ H_2.$$

Assuming that peridotite is mostly composed of olivine, there is 44.4 g of H_2O used for 305 g of olivine, which is about 15% mass. The density of oceanic crust serpentine is 2.53 [*Christensen*, 1978]. If one takes this value for the model of Ceres, there is still some free H_2O remaining after the reaction, which can form a 50 km thick layer (Figure 1).

[47] The thermal history for this model is equivalent to that described for the previous Model 2 except that the thickness of the H_2O layer is much smaller, leading to a factor of two more rapid cooling. More important is the energy involved in the transformation of peridotite into serpentinite. Taking the value of 233 kJ/kg [*Grimm and McSween*, 1989], we find that the total amount of energy is 1.6×10^{26} J. This will produce an increase in temperature of 233 K if one takes a value of 1 kJ/kg/K for the heat capacity. This increase is quite large and would speed up the reaction process. If this temperature increase is added to the temperature profile obtained in the evolution scenario 1 (Figure 3) or to the temperature profile obtained in the core for evolution scenario 2 (Figure 6), temperatures as high as 900 K could be reached in the center of the satellite. These temperatures do not seem large enough to provide melting and formation of an iron-rich core.

3.5.2. Amount of ^{26}Al

[48] There is a trade-off between the amount of ^{26}Al in the CAIs and the duration time: a given amount of ^{26}Al in the kilometer-sized objects can correspond to either large amount of ^{26}Al in the CAIs and long duration time or small amount of ^{26}Al in the CAIs and small duration time. We use the duration time (the time between the formation of CAIs and the beginning of Ceres' accretion from kilometer-sized objects) as a free parameter that determines the amount of short-lived radionuclide-produced energy available once Ceres is formed. We have run models with duration time from 0 to 5 Myr (Figure 9). For duration time of 0 and 1 Myr, the temperature becomes so high that water would vaporize and escape (Figure 9). The scenarios described above assume a duration time of 2.4 Myr. For periods longer than this value, there is a temperature increase related to the decay of the short-lived radionuclides followed by a plateau before temperature raises again due to the decay of the long-lived radionuclides (see curve for t = 5 Myr in Figure 9). If the duration time becomes larger than 8 Myr, then the effect of ^{26}Al becomes smaller than that of the long-lived radionuclides (Figure 2) and its effect is negligible. This range of energy dictates how fast the object heats up and how hot it becomes, but with the large amount of water available, the temperature range possible does not change the general characteristics of the evolution scenarios described above: the more ^{26}Al in the kilometer-sized objects, the faster the ice melts within Ceres. Note that it is not possible to provide enough heat to melt the icy crust because of the conductivity of ice and the relatively cold exterior temperature. Similarly, there is insufficient heat to melt the silicates and form an iron core. However, it is possible that during the accretion period, already differentiated bodies with an iron core accreted and lead to the formation of an iron-rich inner core (Figure 4d). The amount of energy does affect the amount and type of hydrous alteration possible, but even with no short live radioactivity the object heats up more than enough to melt all the water and reach temperatures where mineral alteration reactions occur quickly, in tens to hundreds of years.

3.5.3. Thermal Evolution During Accretion

[49] The present models assume instantaneous accretion from kilometer-sized objects. The thermal evolution during accretion has been investigated previously by *Ghosh et al.* [2003] and *Merk et al.* [2002] for H_2O-free asteroids. Their results show the expected decrease of the maximum temperature for increasing accretion time. If accretion lasted 1 Myr, the difference in the maximum temperature with the instantaneous accretion model is 15% [*Merk et al.*, 2002, Figure 4]. Since the accretion could have lasted less than 0.1 Myr [*Weidenschilling et al.*, 1997], the error would be less than 2%, a difference quite small compared to other uncertainties such as the amount of ^{26}Al.

3.5.4. Surface Temperature

[50] The assumed surface temperature provides the upper boundary condition for the models. A lower temperature is expected since the Sun could have been fainter during the accretion period [*Gaidos*, 2000]. Note that a 30% less bright Sun would cause a 8% lower surface temperature. In evolution scenario 2, this lower surface temperature would increase the thickness of the conductive lid by 3 km and does not change the efficiency of heat transfer by subsolidus convection. For the evolution scenario 1, it would allow a heat flow about 20% larger, but this effect is limited in time and does not affect the long-term evolution and the current internal structure models.

Table 6. Values of the Moment of Inertia for the Models Displayed in Figure 4[a]

	Model 1	Model 2	Model 3	Model 4
Core radius	homogeneous (density = 2.1)	peridotite (density: 3.44)	serpentine (density: 2.54)	iron-core (density = 7.9)
MoI (C/MR^2)	0.4	0.311	0.359	0.304
Love number k_S	1.5	0.793	1.15	0.767
J_2	$31.6\ 10^{-3}$	$16.7\ 10^{-3}$	$24.2\ 10^{-3}$	$15.9\ 10^{-3}$
(a – c), km	38	27	32	26

[a]Models 1 and 4 correspond to Figures 5a and 5d, respectively. Models 2 and 3 were calculated for two different kinds of silicates (Figure 4b). For each moment of inertia, values of the Love number, J2, and difference between equatorial and polar radii can be computed assuming hydrostatic equilibrium. Moment of inertia measurements should be obtained by the DAWN mission (radio science gravity experiment) and will indicate Ceres' internal mass distribution and will give constraints on its thermal evolution. Our interpretation of the measurements of the shape of Ceres (Table 2) shows a difference of 30 km between equatorial and polar radii, between what Models 2 and 3 predict and far from the homogeneous model prediction.

3.5.5. Ammonia

[51] The possible presence of ammonia and likely presence salts has much greater impact on the possible model results. NH_4-bearing compounds have been suggested to explain the 3.1-μm absorption feature in the reflectance spectrum for the surface material [*King et al.*, 1992]. Ceres is in a part of the solar system where such materials might have been incorporated at formation, according to a number of models. Significant presents of these materials would lower the melting point of the liquid water sufficiently (as much as more than 100 K) to extend the lifetime and size of the liquid layer. Salt minerals also reduce the melting point of water, and they likely were created and are present, but they have less effect than ammonia.

3.5.6. Density

[52] The density assumed for the silicate core can be questioned. A larger density for the peridotite type rock that forms the initial silicate of Ceres is possible, say 3810 kg/m^3 [*Bennert and McSween*, 1996] from H chondrites. Such a value would modify very little our models 1 and 2. The main effect is on the thickness of the H_2O layer.

3.5.7. Porosity

[53] As mentioned in evolution scenario 1 (section 3.3), one model (the Callisto's core model described by *Nagel et al.* [2004]) is that of a silicate matrix where pores are filled with ice or water (Figure 4a). Assuming homogeneous interior and a density of 3.44 (from Vesta) for the silicates give a volumetric rock concentration of 45% (porosity of 55%). If the density of silicates is 2.54 (serpentines), the rock concentration is equal to 71% (porosity of 29%), a value that is near the close packing limit [*Torquato et al.*, 2000]. The latter case shows that the internal model described in Figure 4a could be explained by this Callisto's core-like structure. However, the value of the moment of inertia deduced from the shape of Ceres (section 4) suggests that this model is not valid.

4. Predictions and Speculation

[54] A major objective of this study is to predict some of the discoveries that might be made when a spacecraft, such as DAWN, visits Ceres, and to offer some guidance in planning such a mission. One of the obvious measurements to be made is of the gravity field and moment of inertia. Each of the models described above give a different value (Table 6). When the value for J2 is measured and assuming hydrostatic equilibrium, we can compute the value of the moment of inertia in a way similar to that done for the Galilean satellites [*Anderson et al.*, 1996, 1998a, 1998b]. This will put strong constraints on the internal structure of Ceres and allow us to choose among the different scenarios proposed in the present paper.

[55] It is also interesting to note that there is a 30 km difference between the observed equatorial radius and polar radius (Table 2), each of them having an uncertainty on the order of 5 km. This shape difference can be used to estimate the internal mass distribution, using a period for Ceres equal to 9.075 hours [*Lodders and Fegley*, 1998]. If one makes the assumption that Ceres is in hydrostatic equilibrium, the equality of the gravity potential at the pole and at the equator provides a relationship between the equatorial radius (a) and the polar radius (c):

$$f = 1 - \frac{c}{a} = \frac{1}{2}\frac{c}{a}J_2 + J_2\left(\frac{a}{c}\right)^2 + \frac{1}{2}q,$$

where F is called the flattening, J_2 is a constant that depends on the mass radial distribution through the so-called hydrostatic Love number (k_S) and $q = \dfrac{4\pi^2 R^3}{T^2 GM} = 6.31 \cdot 10^{-2}$ is the ratio of centrifugal force to gravitational force. The Love number k_S is related to the moment of inertia and we use the Radau formula to determine it for each of the models depicted in Figure 4. Once ks is obtained, J_2 can be calculated and the flattening is then determined by the equation above.

[56] We have made these calculations for 4 different internal structure models (Table 6). The first case is the homogeneous one, which means $k_S = 1.5$. This value gives $J2 = 3.16\ 10^{-2}$ and a – c = 38 km. The two next cases are the two end-members of Figure 4b, which correspond to a high density and a low density silicate core. The last case is the most differentiated structure described in Figure 4d. In this latter case, $k_S = 0.730$ $J2 = 1.59\ 10^{-2}$ and a–c = 26 km. The radii values from our analysis of Ceres' shape (Table 2) are 485 (equatorial) and 455 km (polar) and the difference is 30 km. This suggests a differentiated Ceres somewhere between the two end-members of the models described in Figure 4b. It is far from the homogeneous case.

[57] One important assumption is hydrostatic equilibrium. This may not be the case for a cold and rigid Ceres (e.g., discussion by *McKinnon* [1997] for Callisto). If DAWN can make good measurements of both the gravity field and the shape of Ceres, these will provide very strong constraints on

the internal structure (hydrostatic assumption, differences in crust density and/or thickness between the equator and the pole) and on the thermal evolution of Ceres.

[58] There must have been dimensional changes in Ceres during evolution. Consider first the water. Ice is less dense than cold water, about an 8% effect in volume. At first Ceres would have shrunk as water formed from ice. As the water warms, however, it would expand, but the water quickly forms a convecting liquid mantle that would remain near the freezing point. Then, as the water froze, Ceres would have expanded. For an object like Ceres, approximately of radius 500 km and 50% water by volume, an 8% change in volume of the water is equivalent to surface extension of approximately the square root of the volume expansion, i.e., on the order of 3%. The silicates also participate in volume changes. Aqueous alteration of silicates produces minerals that are less dense, causing permanent expansion of the object shortly after the ice melted and liquid formed. For alteration of Vesta like peridotite (density about 3.44) to serpentinite (density about 2.55) an increase in volume of about 30% is implied. But this effect is compensated by the smaller volume fraction of water (57% water for a silicate core made of high density silicates compare to 28% water for a silicate core made of serpentines). At first, the reduction in volume by melting ice would quickly be followed by aqueous alteration; quite an active time on Ceres. If there were any initial porosity after formation, one may expect that this would be removed by the differentiation and circulation of water, causing shrinking. At the end of the evolution, the water would freeze, causing expansion. The volume change scenarios are complex, but the salient point is that tectonic features should have formed and the crust disrupted during several phases of Ceres' evolution and evidence of them may be present today.

[59] Major chemistry must have occurred due to the presence of warm circulation water and perhaps ammonia and hydrogen. Initially, silicates, water and carbon compounds probably were present, possibly with ammonia as well. Aqueous alteration of silicates by reactions like those described above must have occurred in the interior during the heating and differentiation, including not only formation of phyllosilicates but also of salts, such as $MgSO_4$, and salt hydrates. Evidence of these products is seen in many Cc meteorites from smaller bodies. Release of hydrogen in some of these reactions would enhance the activity and increase the variety of possible products. Carbon-bearing material in the presence of heat and water can lead to the formation of methane and carbon dioxide. The formation and release of H_2 may have several consequences. Chemical processes involving H_2 and CO_2 may lead to the formation of clathrates, which are stable in the temperature-pressure domain at the silicate/liquid interface. This suggests that chemical reactions could have existed and formed molecules of interest to exobiology studies.

[60] Surface expressions of the internal evolution should be evident. The surface 10 km or so apparently cannot be melted using these models and so might still contain a sample of the initial material forming Ceres. However, a thin rock-rich crust is probably unstable overlaying a less dense liquid water layer and it would tend to break up and the pieces sink, probably soon after the liquid water mantle formed in the first tens of Myr after formation. Heavy bombardment would aid this process. Where this happened, a new solid crust would quickly freeze out, but the primitive material would be lost from the surface and mixed into the mantle. This, however, would bring chemical evidence of interior processes to the surface, as would the tectonic activity driven by convection and dimensional changes as well as gas and water volcanism.

[61] When some of these materials formed by chemical processes (clathrates, superheated water, CO_2) were brought near the surface and into a lower pressure environment, they would volatilize and could produce explosive release of gases. Thus gas-driven volcanism might have occurred on Ceres, bringing considerable quantities of altered materials to the surface and creating surface expressions that DAWN might detect. This process has been discussed for small bodies, including prediction of explosive disintegration of the object [*Grimm and McSween*, 1989; *Wilson et al.*, 1999]. For larger objects, like Ceres, the water vapor horizon apparently is not easily reached (Figure 3) due to the effect of pressure on the vapor horizon, at least globally, but on smaller scales and near the surface, this should lead to gas volcanism, surface rupturing, especially considering the likely tectonic activity, and significant transport of materials to the surface.

5. Conclusions and Observations

[62] Ceres appears to be a complicated object, in some ways similar to the outer Galilean satellites. With so much water present and the energy to distribute it in liquid form, Ceres probably experienced complex chemistry at least in its interior, probably involving organic materials. It is further likely that expressions of these processes and the materials made it to the surface, at least in places. DAWN may well discover and analyze these.

[63] It is instructive to compare Ceres' current density and probable state with that for some other nearby objects (Table 3). As we see from the models, Ceres likely retained much of its original water but this water became redistributed inside Ceres and a significant portion probably was taken up in the mineralization processes. Thus Ceres may be in a similar state as is Ganymede or Callisto but with slightly less water. Europa and to some extent Ganymede have an additional energy source (tidal), with Europa being much more evolved. Callisto had little or no tidal heating and so may have evolved more like Ceres, but Callisto either had more water at its origin (further out in the solar system) or lost less of it (larger).

[64] Vesta is much denser, dryer and has extensively melted. Pallas, being denser, also seems to have evolved further and lost more water or it may have had less to start. A major question is why such different objects as Ceres, Vesta and Pallas, all protoplanets, could have evolved so differently yet so close together in the Solar System [cf. *Matson et al.*, 1976]. The key seems to be the water content. Without a large amount of water in the evolving body, the heat cannot be absorbed by the latent heat of ice and it cannot be convected away by the liquid water mantle and crustal ice. This can lead to melting of silicates and a Vesta-like end product. One possibility is that each of these three objects formed from earlier small objects that formed at

different times, earlier meaning more heating from short-lived radionuclides and more loss of water.

[65] **Acknowledgments.** We acknowledge useful conversations with many colleagues, including Edward Scott, Alexander Krot, Klaus Keil, Jeffrey Bell, and Torrence Johnson. We thank T. Johnson for a careful reading of the manuscript. This article was prepared in part while T. B. McCord was in residence as Distinguished Visiting Professor at the University of Nantes, France. This work was supported in part by NASA Cosmochemistry Program grant NAG 5-10514 and by INSU Programme National de Planétologie. This is University of Hawaii publication 1346 (HIGP) and 6470 (SOEST).

References

A'Hearn, M. F., and P. D. Feldman (1992), Water vaporization on Ceres, *Icarus*, *98*, 54–60.

Allegre, C. J., G. Manhes, and C. Gopel (1995), The age of the Earth, *Geochim. Cosmochim. Acta*, *59*, 1445–1456.

Anderson, J. D., E. L. Lau, W. L. Sjorgren, G. Schubert, and W. B. Moore (1996), Gravitational constraints on the internal structure of Ganymede, *Nature*, *384*, 541–543.

Anderson, J. D., G. Schubert, R. A. Jacobson, E. L. Lau, W. B. Moore, and W. L. Sjogren (1998a), Distribution of rock, metals and ices in Callisto, *Science*, *280*, 1573–1576.

Anderson, J. D., G. Schubert, R. A. Jacobson, E. L. Lau, W. B. Moore, and W. L. Sjogren (1998b), Europa's differentiated internal structure: Inferences from four Galileo encounters, *Science*, *281*, 2019–2022.

Bennert, M. E., and H. Y. McSween Jr. (1996), Revised model calculations for the thermal histories of ordinary chondrite parent bodies, *Meteorit. Planet. Sci.*, *31*, 783–792.

Britt, D. T., and G. J. Consolmagno (2000), Asteroid bulk density, *Bull. Am. Astron. Soc.*, *32*(3), abstract 7.02.

Britt, D. T., D. Yeomans, K. Housen, and G. Consolmagno (2002), Asteroid density, porosity, and structure, in *Asteroids III*, edited by W. F. Bottke Jr. et al., pp. 485–500, Univ. of Ariz. Press, Tucson.

Canup, R. (2004), Origin of terrestrial planets and the Earth-Moon system, *Phys. Today*, *57*, 56–62.

Chapman, C. R. (1975), The collisional evolution of carbonaceous and chemically-differentiated asteroids, *Bull. Am. Astron. Soc.*, *7*, 376.

Chapman, C. R. (1976), Interpretation of new asteroid spectrophotometry, *Bull. Am. Astron. Soc.*, *8*, 460.

Chapman, C. R., and J. W. Salisbury (1973), Comparison of meteorite and asteroid spectral reflectivities, *Icarus*, *19*, 507–522.

Chapman, C. R., T. B. McCord, and T. V. Johnson (1973), Asteroid spectral reflectivities, *Astron. J.*, *78*, 126–140.

Christensen, N. (1978), Ophiolite, seismic velocities and oceanic crustal structure, *Tectonophysics*, *47*, 131–157.

Clayton, R. N., and T. K. Mayeda (1984), The oxygen isotope record in Murchison and other carbonaceous chondrites, *Earth Planet. Sci. Lett.*, *67*, 151–161.

Clayton, R. N., and T. K. Mayeda (1999), Oxygen isotope studies of carbonaceous chondrites, *Geochim. Cosmochim. Acta*, *63*, 2089–2104.

Deschamps, F., and C. Sotin (2001), Thermal convection in the outer shell of large icy satellites, *J. Geophys. Res.*, *106*, 5107–5121.

Dotto, E., et al. (2000), ISO results on bright Main Belt asteroids: PHT-S observations, *Astron. Astrophys.*, *358*, 1133–1141.

Drummond, J. D., R. Q. Fugate, and J. C. Christou (1998), Full adaptive optics images of asteroids Ceres and Vesta: Rotational poles and triaxial ellipsoid dimensions, *Icarus*, *132*, 80–99.

DuFresne, E. R., and E. Anders (1962), On the chemical evolution of the carbonaceous chondrites, *Geochim. Cosmochim. Acta*, *26*, 1085–1114.

Encyclopædia Britannica (2004), Giuseppe Piazzi, Chicago, Ill. (Available at http://www.britannica.com/search?query=Giuseppe+Piazzi&ct=)

Fanale, F. P., and J. R. Salvail (1989), The water regime of asteroids 1 Ceres, *Icarus*, *82*, 97–110.

Feierberg, M. A., L. A. Lebofsky, and H. P. Larson (1981), Spectroscopic evidence for aqueous alteration products on the surfaces of low-albedo asteroids, *Geochim. Cosmochim. Acta*, *45*, 971–981.

Gaffey, M. J., and T. B. McCord (1978), Asteroid surface materials: Mineralogical characterizations from reflectance spectra, *Space Sci. Rev.*, *21*, 555–628.

Gaidos, E. J. (2000), The faint young Sun paradox: An observational test of an alternative solar model, *Geophys. Res. Lett.*, *27*, 501–503.

Ghosh, A., S. J. Weidenschilling, and H. Y. McSween (2003), Importance of the accretion process in asteroid thermal evolution: 6 Hebe as an example, *Meteorit. Planet. Sci.*, *38*, 711–724.

Grasset, O., and C. Sotin (2000), On the internal structure and dynamics of Titan, *Planet. Space Sci.*, *48*, 617–636.

Greenberg, R., and C. R. Chapman (1983), Asteroids and meteorites: Parent bodies and delivered samples, *Icarus*, *55*, 455–481.

Grimm, R. E., and H. Y. McSween (1989), Water and the thermal evolution of carbonaceous chondrite parent bodies, *Icarus*, *82*, 244–280.

Hilton, J. L. (1999), US Naval Observatory ephemeredes of the largest asteroids, *Astron. J.*, *117*, 1077–1086.

Johnson, T. V., and J. D. Anderson (2003), Galileo's encounter with Amelthea, paper presented at EGS-AGU-EUG Joint Assembly, Eur. Geophys. Soc., Nice, France.

Johnson, T. V., and F. P. Fanale (1973), Optical properties of carbonaceous chondrites and their relationship to asteroids, *J. Geophys. Res.*, *78*, 8507–8578.

Jones, T. D., L. A. Lebofsky, and J. S. Lewis (1988), The 3 μm hydrated silicate signature on C class asteroids: Implications for origins of outer belt objects, *Lunar Planet. Sci.*, *XIX*, 567–568.

Jones, T. D., L. A. Lebofsky, J. S. Lewis, and M. S. Marley (1990), The composition and origin of the C, P, and D asteroids: Water as a tracer of thermal evolution in the outer belt, *Icarus*, *88*, 172–192.

Keil, K. (2002), Geological history of asteroid 4 Vesta: The "smallest terrestrial planet," in *Asteroids III*, edited by W. F. Bottke Jr. et al., pp. 573–584, Univ. of Ariz. Press, Tucson.

King, T. V. V., R. N. Clark, W. M. Calvin, D. M. Sherman, and R. H. Brown (1992), Evidence for ammonium—Bearing minerals on Ceres, *Science*, *255*, 1551–1553.

Kivelson, M. G., K. K. Khurana, D. J. Stevenson, L. Bennett, S. Joy, C. T. Russel, R. J. Walker, and C. Polanskey (1999), Europa and Callisto: Induced or intrinsic fields in a periodically varying plasma environment, *J. Geophys. Res.*, *104*, 4609–4625.

Kivelson, M. G., K. K. Khurana, and M. Volwerk (2002), The permanent and inductive magnetic moments of Ganymede, *Icarus*, *157*, 507–522.

Krot, A. N., A. J. Brearley, A. A. Ulyanov, V. V. Biryukov, T. D. Swindle, K. Keil, D. W. Mittlefehldt, E. R. D. Scott, R. N. Clayton, and T. K. Mayeda (1999), Mineralogy, petrography, bulk chemical, iodine-xenon, and oxygen-isotopic compositions of dark inclusions in the reduced CV3 chondrite Efremovka, *Meteorit. Planet. Sci.*, *34*, 67–90.

Krot, A. N., K. Keil, C. Goodrich, M. K. Weisberg, and E. R. D. Scott (2003), Classification of meteorites, in *Treatise on Geochemistry*, edited by K. K. Turekian and A. Davis, chap. 5, Elsevier, New York.

Lagerkvist, C. I., and P. Magnusson (1990), Analysis of asteroid light curves II—Phase curves in a generalized HG-system, *Astron. Astrophys. Suppl. Ser.*, *86*, 119–165.

Larson, H. P., M. A. Feierberg, U. Fink, and H. A. Smith (1979), Remote spectroscopic identification of carbonaceous chondrite mineralogies: Applications to Ceres and Pallas, *Icarus*, *39*, 257–271.

Lebofsky, L. A. (1978), Asteroid 1 Ceres: Evidence for water of hydration, *Mon. Not. R. Astron. Soc.*, *182*, 17–21.

Lebofsky, L. A. (1980), Infrared reflectance spectra of asteroids: A search for water of hydration, *Astron. J.*, *85*, 573–585.

Lebofsky, L. A., and J. R. Spencer (1989), Radiometry and thermal modeling of asteroids, in *Asteroids II*, edited by R. P. Binzel, T. Gehrels, and J. S. Matthews, pp. 128–147, Univ. of Ariz. Press, Tucson.

Lebofsky, L. A., M. A. Feierberg, A. T. Tokunaga, H. P. Larson, and J. R. Johnson (1981), The 1.7- to 4.2-μm spectrum of asteroid 1 Ceres: Evidence for structural water in clay minerals, *Icarus*, *48*, 453–459.

Lee, T., D. Papanastassiou, and G. J. Wasserburg (1976), Demonstration of ^{26}Mg excess in Allende and evidence for ^{26}Al, *Geophys. Res. Lett.*, *3*, 109–112.

Leshin, L. A., A. E. Rubin, and K. D. McKeegan (1997), The oxygen isotopic composition of olivine and pyroxene from CI chondrites, *Geochim. Cosmochim. Acta*, *61*, 835–845.

Lodders, K., and B. Fegley (1998), *The Planetary Scientist's Companion*, Oxford Univ. Press, New York.

MacPherson, G. J., A. M. Davis, and E. K. Zinner (1995), The distribution of 26Al in the early solar system—A reappraisal, *Meteoritics*, *30*, 365–386.

Manga, M., and D. Weeraratne (1999), Experimental study of a non-Boussinesq Rayleigh-Bénard convection at high Rayleigh and Prandtl numbers, *Phys. Fluid*, *11*, 2969–2976.

Mason, B. (1971), *Handbook of Elemental Abundances in Meteorites*, Gordon and Breach, New York.

Matson, D. L., F. P. Fanale, T. V. Johnson, and G. J. Veeder (1976), Asteroids, and comparative planetology, *Geochim. Cosmochim. Acta Suppl.*, *7*, 3603–3627.

McCord, T. B., and M. J. Gaffey (1974), Asteroids: Surface composition from reflection spectroscopy, *Science*, *186*, 352–355.

McCord, T. B., J. B. Adams, and T. V. Johnson (1970), Asteroid Vesta: Spectral reflectivity and compositional implications, *Science*, *168*, 1445–1447.

McKinnon, W. B. (1997), Mystery of Callisto: Is it differentiated?, *Icarus*, *130*, 540–543.

McSween, H. Y., Jr., A. Ghosh, R. E. Grimm, L. Wilson, and E. D. Young (2002), Thermal evolution models of asteroids, in *Asteroids III*, edited by W. F. Bottke Jr. et al., pp. 559–571, Univ. of Ariz. Press, Tucson.

Merk, R., D. Breuer, and T. Spohn (2002), Numerical modeling of ^{26}Al-induced radioactive melting of asteroids considering accretion, *Icarus*, *159*, 183–191.

Michalak, G. (2000), Determination of asteroid masses I. (1) Ceres, (2) Pallas and (4) Vesta, *Astron. Astrophys*, *360*, 363–374.

Millis, R. L., et al. (1987), The size, shape, density and albedo of Ceres from its occultation of BD + 8 deg 471, *Icarus*, *72*, 507–518.

Nagel, K., D. Breuer, and T. Spohn (2004), A model for the interior structure, evolution, and differentiation of Callisto, *Icarus*, *169*, 402–412.

Parker, J. W., S. A. Stern, P. C. Thomas, M. C. Festou, W. J. Merline, and E. F. Young (2002), Analysis of the first disk-resolved images of Ceres from ultraviolet observation with the Hubble Space Telescope, *Astron. J.*, *123*, 549–557.

Piazzi, G. (1802), Della scoperta del nuovo planeta Cerere Ferdinandea, Palermo Observ., Palermo, Italy.

Saint-Pe, O., M. Combes, and F. Rigaut (1993), Ceres surface properties by high-resolution imaging from Earth, *Icarus*, *105*, 271–281.

Schubert, J., and D. L. Matson (1979), Masses and densities of asteroids, in *Asteroids*, edited by T. Gehrels, pp. 84–97, Univ. of Ariz. Press, Tucson.

Solomatov, V. S. (1995), Scaling of temperature- and stress-dependent viscosity convection, *Phys. Fluids*, *7*, 266–274.

Sotin, C., and G. Tobie (2004), Internal structure and dynamics of the large icy satellites, *C. R. Acad. Sci. Phys.*, *5*, 769–780.

Sotin, C., O. Grasset, and S. Beauchesne (1997), Thermodynamic properties of high pressure ices: Implications for the dynamics and internal structure of large icy satellites, in *Solar System Ices*, edited by B. Schmitt et al., pp. 79–96, Springer, New York.

Srinivasan, G., J. N. Goswami, and N. Bhandari (1999), ^{26}Al in eucrites Piplia Kalan: Plausible heat source and formation chronology, *Science*, *284*, 1348–1350.

Standish, E. M. (2001), JPL interoffice memorandum, *312, F-01-006*, Jet Propul. Lab., Pasadena, Calif., 11 April.

Standish, E. M., and R. W. Hellings (1989), A determination of the masses of Ceres, Pallas, and Vesta from their perturbations upon the orbit of Mars, *Icarus*, *80*, 326–333.

Swindle, T. D., M. W. Caffee, and C. M. Hohenberg (1988), Iodine-xenon studies of Allende inclusions Eggs and the Pink Angel, *Geochim. Cosmochim. Acta*, *52*, 2215–2227.

Tedesco, E. F. (1989), Asteroid magnitudes, UBV colors, and IRAS albedos and diameters, in *Asteroids II*, edited by R. P. Binzel, T. Gehrels, and J. S. Matthews, pp. 1090–1138, Univ. of Ariz. Press, Tucson.

Thomas, P. C., J. Veverka, and S. Dermott (1986), Small satellites, in *Satellites*, edited by J. A. Burns and M. S. Matthews, pp. 802–835, Univ. of Ariz. Press, Tucson.

Thomas, P. C., R. P. Binzel, M. J. Gaffey, B. H. Zellner, A. D. Storrs, and E. N. Wells (1997), Vesta: Spin pole, size and shape from HST images, *Icarus*, *128*, 88–94.

Tobie, G., G. Choblet, and C. Sotin (2003), Tidally heated convection: Constraints on Europa's ice shell thickness, *J. Geophys. Res.*, *108*(E11), 5124, doi:10.1029/2003JE002099.

Torquato, S., T. M. Truskett, and P. G. Debenedetti (2000), Is random close packing of spheres well defined?, *Phys. Rev. Lett.*, *84*, 2064–2067.

Turcotte, D., and G. Schubert (1981), *Geodynamics*, 450 pp., John Wiley, Hoboken, N. J.

Viateau, B., and M. Rapaport (1998), The mass of (1) Ceres from its gravitational perturbations on the orbits of 9 asteroids, *Astron. Astrophys.*, *334*, 729–735.

Weidenschilling, S. J., D. Spaute, D. R. Davis, F. Marzari, and K. Ohtsuki (1997), Accretional evolution of a planetesimal swarm, *Icarus*, *128*, 429–455.

Wilson, L., K. Keil, L. B. Browning, A. N. Krot, and W. Bourcier (1999), Early aqueous alteration, explosive disruption, and reprocessing of asteroids, *Meteorit. Planet. Sci.*, *34*, 541–557.

Young, E. D., R. D. Ash, P. England, and D. Rumble III (1999), Fluid flow in chondrite parent bodies: Deciphering the compositions of planetesimals, *Science*, *286*, 1331–1335.

T. B. McCord, Hawaii Institute of Geophysics and Planetology, University of Hawaii, 2525 Correa Road, Honolulu, HI 96822, USA. (mccordtb@aol.com)

C. Sotin, Laboratory de Planetologie et Geodynamique, University of Nantes, Nantes, France.